

Optimization of Focal Position of Ultrasonic Beam in Measurement of Small Change in Arterial Wall Thickness

Masaru WATANABE* and Hiroshi KANAI†

Department of Electrical Engineering, Tohoku University Graduate School of Engineering, Aramaki-aza-Aoba 05, Aoba-ku, Sendai 980-8579, Japan

(Received November 23, 2000; accepted for publication February 5, 2001)

We have previously developed a method for measurement of a small change in thickness of the arterial wall during a single cardiac cycle [H. Kanai, M. Sato, Y. Koiwa and N. Chubachi: IEEE Trans. UFFC **43** (1996) 791]. The resultant change in thickness is shown to be useful for the *in vivo* assessment of the regional elasticity of the arterial wall. Although the accuracy of the measurement of the change in thickness is found to be within $1\ \mu\text{m}$, it is affected by the interference of ultrasonic pulses. In this study, we simulate the propagation of ultrasonic pulses transmitted and received by a linear probe. In the simulation experiments, the ultrasonic pulses generated by a computer are reflected by a tube, which has a small change in wall thickness of $10\ \mu\text{m}$. The optimum focal position of the ultrasonic beam is determined by evaluating the root-mean-square (rms) error in the measured change in thickness.

KEYWORDS: atherosclerosis, change in thickness of arterial wall, computer simulation, interference, focus

1. Introduction

The increase in the number of individuals suffering from myocardial or cerebral infarction, both of which are mainly caused by atherosclerosis, has become a serious clinical problem. It is therefore important to diagnose atherosclerosis at an early stage. However, to date, there is no method available for the detection of minute changes in the elasticity of arterial walls due to early-stage atherosclerosis.

We have developed a method for evaluating the elasticity in each local region within about $400\ \mu\text{m}$ from the arterial wall^{1,2)} to diagnose its vulnerability to atherosclerotic plaque. The small change in thickness of the arterial wall due to the heartbeat is accurately measured in each local region around the focal area of the ultrasonic beam. From the resultant change in thickness, the local strain and the elasticity of the arterial wall are noninvasively evaluated. By scanning the ultrasonic beam, the spatial distribution of the elasticity is also obtained.

In this measurement, however, the accuracy is affected by the interference of ultrasonic pulses. Figure 1 shows the measured waveform reflected from a rubber plate in a water tank. The employed transmitted ultrasonic pulse is $7.5\ \text{MHz}$ and $1.0\ \mu\text{s}$ long. In Fig. 1, the thicknesses of the rubber plates are $0.40\ \text{mm}$ and $0.65\ \text{mm}$. The anterior surface and posterior surface can be separated only as shown in Fig. 1(b). In Fig. 1(a), the two surfaces cannot be separated due to the interference of reflective waves. If the optimum focal position is employed, the effects of the interference will be reduced. Currently, in commercial ultrasonic diagnostic equipment, multiple focal locations are employed for multiple transmissions, but the pulse repetition frequency (PRF) is reduced. Our research objective is to determine the spatial distribution of the elasticity for a wider region and in more detail. For this purpose, the PRF cannot be reduced. In this study, therefore, we simulate an *in vivo* measurement of the small change in thickness in the arterial wall during a single cardiac cycle. From the simulation experiments, the focal position which is optimized to reduce the effects of the interference of ultrasonic

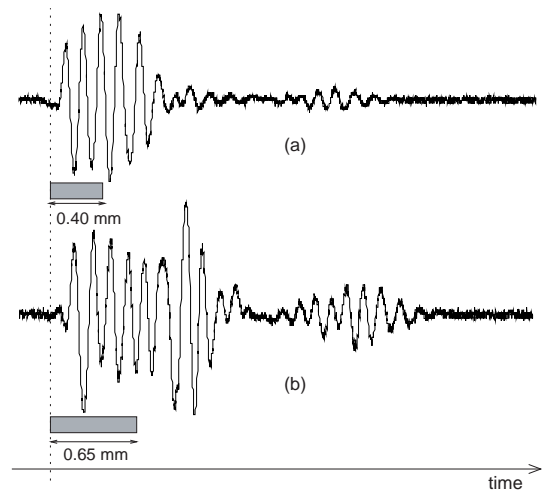


Fig. 1. The measured waveform reflected from a rubber plate in a water tank. (a) The thickness of the rubber plate is $0.40\ \text{mm}$. (b) The thickness of the rubber plate is $0.65\ \text{mm}$.

pulses is chosen.

2. Principle of Computer Simulation for Measurement of Small Change in Thickness

In the simulation, an arbitrarily shaped reflector in the $x-z$ plane of Fig. 2, which corresponds to a tube, is divided into small scatterers. An electrical scanning linear probe with $(2N+1)$ elements in Fig. 2(a) is employed. The distance from the n th element ($-N \leq i \leq N$) to the focal point at a depth of $z = d_f$ is given by $\sqrt{d_f^2 + (n \cdot \Delta h)^2}$, where Δh denotes the element pitch. Thus, in order to focus the ultrasonic pulses transmitted from $(2N+1)$ elements on the focal point, the following delay time t_n is added to the delay line connected to the n th element:

$$t_n = \frac{\sqrt{d_f^2 + (N \cdot \Delta h)^2}}{c_0} - \frac{\sqrt{d_f^2 + (n \cdot \Delta h)^2}}{c_0}, \quad (1)$$

where c_0 is the sound speed. The incidence angle, θ_{ni} , from the n th element of the probe to the i th small scatterer on the

*E-mail address: watanabe@us.ecei.tohoku.ac.jp

†E-mail address: hkanai@us.ecei.tohoku.ac.jp

surface of the reflector is determined by the regional shape of the reflector and the geometrical relationship between the n th element and the reflector shown in Fig. 2(b). The ultrasonic pulse is reflected with the same angle θ_{ni} , as shown in Fig. 2(b). The receiving angle φ_{im} from the i th small scat-

terer to the m th element in Fig. 2(c) is determined in the same manner. Thus, the RF ultrasonic wave $y_m(t)$ received at the m th element is given by the summation of the reflective waves at all scatterers $\{i\}$ for the transmitted signal with an angular frequency $\omega_0 = 2\pi f_0$ radiated from all elements as follows:

$$y_m(t) = \sum_{-N \leq n \leq N} W(t - t_n) \cdot \sin \omega_0(t - t_n) * \left(\sum_i \delta(t - t'_{ni}) \cos \theta_{ni} * \delta(t - t''_{im}) \cdot \cos \theta_{im} \right), \quad (2)$$

where t'_{ni} and t''_{im} denote the traveling time from the n th element to the i th small scatterer and that from the i th small scatterer to the m th element, respectively, $W(t)$ is the Hanning window which is four times the wavelength λ , $\delta(t)$ is the Dirac delta function, and $*$ denotes the convolution operation. The terms $\cos \theta_{ni}$ and $\cos \theta_{im}$ denote the widths of the i th small scatterer and the m th element, respectively, observed from the propagating ultrasonic beam. The output signal $y(t)$ of the probe, with the delayed summation of $\{y_m(t)\}$, is given by

$$y(t) = \sum_{-N \leq m \leq N} y_m(t) * \delta(t - t_m). \quad (3)$$

The instantaneous position of the object is changed according to the assumed change in thickness. By applying the phase tracking method³⁾ to the quadrature-demodulated signal of $y(t)$, the change in thickness $\Delta d(t)$ of the object is estimated.

In this simulation experiment, the number of elements, $2N + 1$, is 17 with the element pitch of $\Delta h = 150 \mu\text{m}$. The spacing of small scatterers on the reflector is $10 \mu\text{m}$ between points. The reflector is a tube with an inner radius of 3.4 mm and an outer radius of 4 mm. Its cross-sectional view on the $x-z$ plane is shown in Fig. 3.

The maximum value Δd_{max} of the change in arterial wall thickness during a single cardiac cycle with the period $1/f_{\text{rot}}$ is assumed to be $10 \mu\text{m}$. Under this condition, the velocity of the inner surface, $v_i(t)$, of the tube and the velocity of the

outer surface, $v_o(t)$, are given by

$$v_i(t) = (\alpha + 1)\pi \Delta d_{\text{max}} f_{\text{rot}} \sin(2\pi f_{\text{rot}} t) \quad (4)$$

$$v_o(t) = \alpha \pi \Delta d_{\text{max}} f_{\text{rot}} \sin(2\pi f_{\text{rot}} t), \quad (5)$$

where α determines the ratio of $v_i(t)$ to $v_o(t)$.

In the following experiments, $\alpha = 0.5$, f_{rot} is 1.5 Hz, $f_0 = 7.5 \text{ MHz}$, $c_0 = 1,480 \text{ m/s}$, and $\text{PRF} = 1 \text{ kHz}$. The change in thickness, $\Delta d(t)$, is obtained from the integration of the difference between the estimates of $\hat{v}_i(t)$ and $\hat{v}_o(t)$ as follows:

$$\Delta d(t) = \int_0^t (v_i(t) - v_o(t)) dt. \quad (6)$$

3. Results of Simulation Experiment on the Measurement of a Tube

Figure 4 shows a B-mode image reconstructed from the simulated RF signal $y(t)$ for each position k of the employed

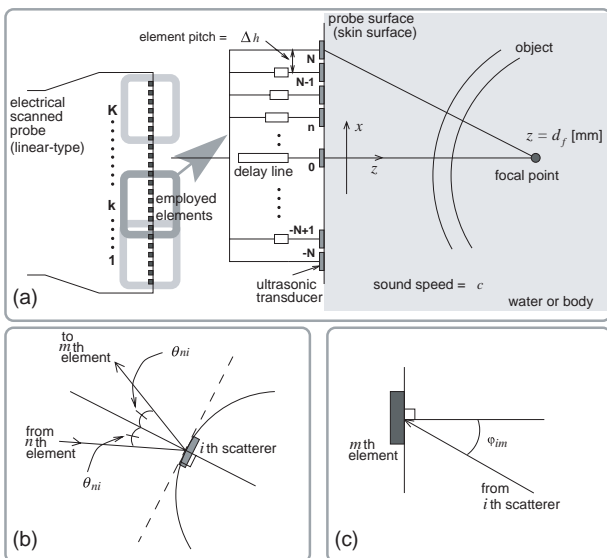


Fig. 2. The electric scanned linear probe is employed by the computer simulation. (a) The simulation system, (b) the reflection on the i th scatterer, and (c) the reception on the m th element.

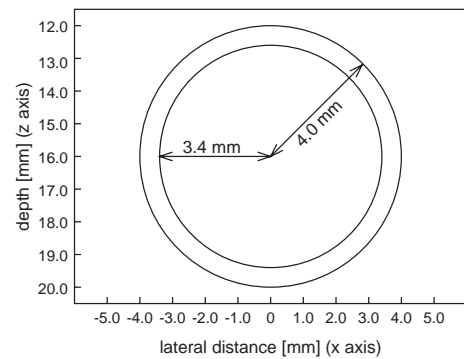


Fig. 3. The shape of a tube employed in the computer simulation.

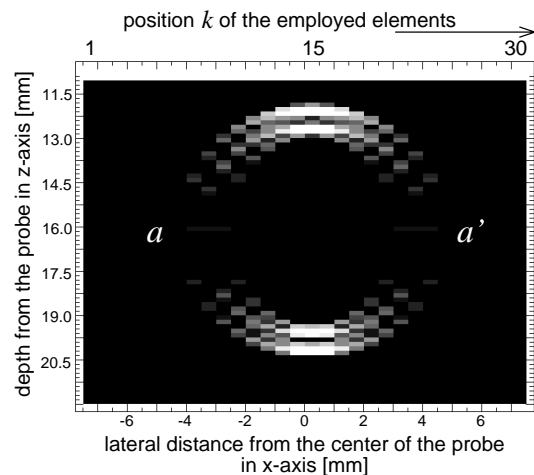


Fig. 4. The B-mode image reconstructed from the simulated RF signals $y(t)$ in the simulation experiment.

elements in Fig. 2(a). The distance between the adjacent positions is 0.5 mm. The received signal $y(t)$ reflected at both sides (a and a' in Fig. 4) of the tube is small in amplitude because the values of $\cos \theta_{ni}$ in eq. (2) are small at these points. These phenomena are also shown in the actual B-mode image in Fig. 5 in detected by commercial ultrasonic diagnostic equipment (Toshiba SSH-140A, $f_0 = 7.5$ MHz).

Figure 6 shows the actual values and their estimated results in the simulation experiments, where the distance d_f of the focal point from the probe is assumed to be 15 mm. The estimates of the change in thickness, $\Delta \hat{d}(t)$, of the anterior wall in Fig. 6(e) and the posterior wall in Fig. 6(f) are similar to the assumed waveforms.

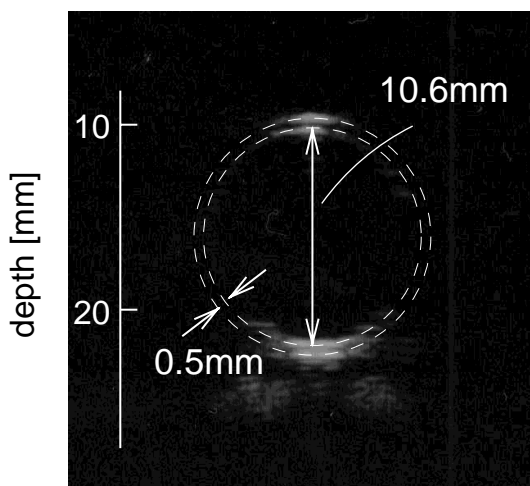


Fig. 5. The actual B-mode image of a silicone rubber tube detected by the ultrasonic diagnostic equipment. The actual cross-sectional shape is shown by broken lines. The silicone tube is almost the same size as that employed in the simulation experiment.

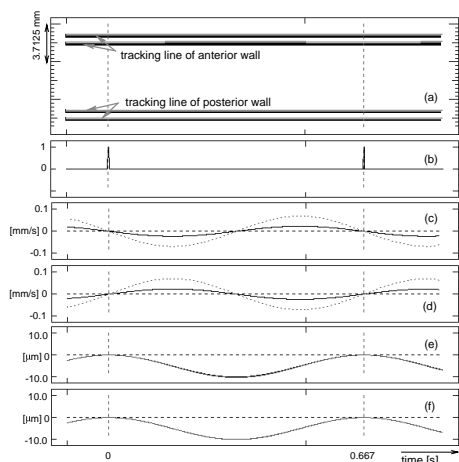


Fig. 6. The result of the measurement with a tube by computer simulation. (a) M-mode image, (b) timing pulse train showing one cardiac cycle, (c) velocity estimates, $\hat{v}_i(t)$ (dashed line) and $\hat{v}_o(t)$ (solid line), of the anterior wall, (d) velocity estimates, $\hat{v}_i(t)$ (dashed line) and $\hat{v}_o(t)$ (solid line), of the posterior wall, (e) the actual value $\Delta d(t)$ of the change in thickness of the anterior wall, and its estimate $\Delta \hat{d}(t)$, (f) the actual value $\Delta d(t)$ of the change in thickness of the posterior wall, and its estimate $\Delta \hat{d}(t)$.

4. Optimum Focal Position Determined by Simulation Experiments

For the comparison between the change in thickness, $\Delta \hat{h}(t)$, estimated from the RF signal $y(t)$ generated in the simulation experiment described above and the actual change in thickness, $\Delta h(t)$, which is assumed in the simulation experiment, the following rms error, e_{rms} , is defined during one cardiac cycle T:

$$e_{\text{rms}} = \sqrt{\frac{1}{T} \int_0^T \{\Delta h(t) - \Delta \hat{h}(t)\}^2 dt}. \quad (7)$$

For various values of the focal position d_f , the rms error e_{rms} is obtained for each of the anterior and posterior walls, as shown in Fig. 7, where the distance from the probe to the outer surface of the anterior wall is fixed at 11 mm. It is found that for both walls the optimum focal position d_f is about 12 mm from the probe, which corresponds to the position between the anterior wall and the center depth of the tube.

Moreover, the characteristics of the rms error for the anterior wall differ from those of the posterior wall. The reason for these differences is considered to be as follows. There are three main types of walls, as shown in Fig. 8, that is, convex (anterior), concave (posterior), and flat walls. For various values of the focal position d_f , the rms error e_{rms} is obtained for the three kinds of walls shown in Fig. 9.

In the measurement of the anterior wall, high accuracy is obtained by setting the focal position d_f just on the reflector surface. In the measurement of the posterior wall, on the other hand, higher accuracy is obtained by setting the focal position d_f nearer than the depth of the reflector surface, which is similar to the phenomenon where the focal point is situated at the front of the wall if the wall has parabolic curvature.

Thus, the optimum focal position d_f in the posterior wall is set to be slightly nearer than the reflector surface. The dis-

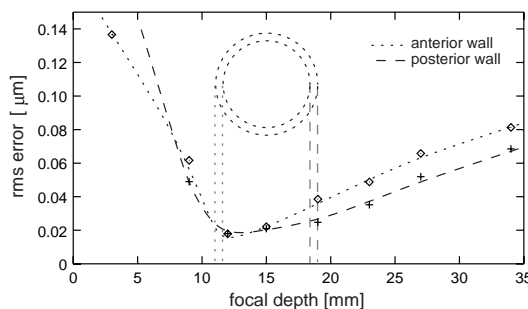


Fig. 7. The rms error in the estimation of the change in thickness of the tube with the center depth of 15 mm, the outer radius of 4.0 mm, and the inner radius of 3.4 mm.

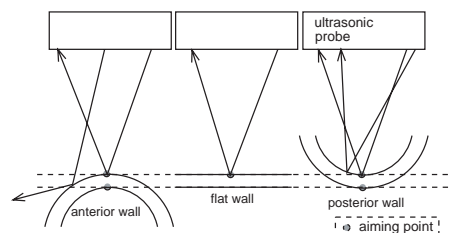


Fig. 8. Three reflector types: the convex (anterior), flat, and concave (posterior) walls.

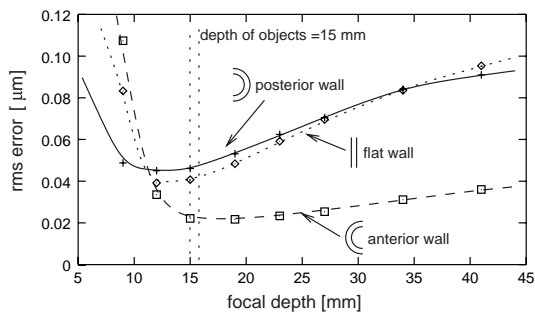


Fig. 9. The rms error of the three types of reflectors with a depth of 15 mm.

tance from the reflector position to the optimum focal point depends on the curvature of the tube.

5. Conclusions

From the simulation experiments, we have evaluated the accuracy of the measurement of the small change in arterial

wall thickness for various focal positions. Based on the results, we have determined the optimum focal position for each measurement.

- 1) H. Kanai, H. Hasegawa, N. Chubachi, Y. Koiwa and M. Tanaka: IEEE Trans. UFFC **44** (1997) 752.
- 2) H. Kanai, H. Hasegawa, N. Chubachi and Y. Koiwa: Electron. Lett. **33** (1997) 340.
- 3) H. Kanai, M. Sato, Y. Koiwa and N. Chubachi: IEEE Trans. UFFC **43** (1996) 791.
- 4) H. Hasegawa, H. Kanai, N. Hoshimiya, N. Chubachi and Y. Koiwa: Jpn. J. Appl. Phys. **37** (1998) 3101.
- 5) H. Kanai, K. Sugimura, Y. Koiwa and Y. Tsukahara: Electron. Lett. **35** (1999) 949.